Supporting information:

A microfluidic strategy for accessing the thermal conductivity of liquids at different temperatures

Rosa Moreno Jimenez[1,2], Benoit Creton[1*], Claire Marliere[1], Lionel Teule-Gay[2], Olivier Nguyen[2], Samuel Marre[2*]

[1]IFP Energies nouvelles, 1 et 4 avenue de Bois-Préau, 92852 Rueil-Malmaison, France.

[2]CNRS, Univ. Bordeaux, ICMCB, UMR 5026, F-33600 Pessac, France

---

ESI-1: Microfabrication procedure

Microchannel fabrication process. The microchannel was etched on a silicon substrate surface following the standard photolithography and etching protocol, previously described [1]. The process starts with the use of a silicon wafer, covered with a 500 nm layer of SiO_2. A positive photoresist resin (S1818 - Shipley) is spin-coated at 1200 rpm for 30 s, resulting in a photoresist layer of 4 µm in thickness on the silicon surface. The silicon substrate is then placed on a hot plate, and the photoresist undergoes a pre-baking step for 4 min at 115°C. The wafer is then exposed through the photomask to ultraviolet (UV) exposure using a LED UV-masking insulator (UV-KUB2, KLOE) at 40 mW/cm^2 (λ = 365 nm) for 45 s. The exposed photoresist resin is then developed using a MF319 developer (Shipley) for 30 s. The substrate is rinsed with water, and the wafer is finally post-baked for a final 6 min at 115°C to ensure its strength after the development stage. Once the mask is printed in negative on the silicon substrate, the unprotected SiO_2 layer is first removed using a buffered oxide etchant (BOE) solution. Then, the photoresist layer is removed using acetone and the silicon is finally etched using a tetramethylammonium hydroxide (25 wt% in water) solution at 85°C for 70 min resulting in a trapezoidal crossed section channel 60 µm deep.

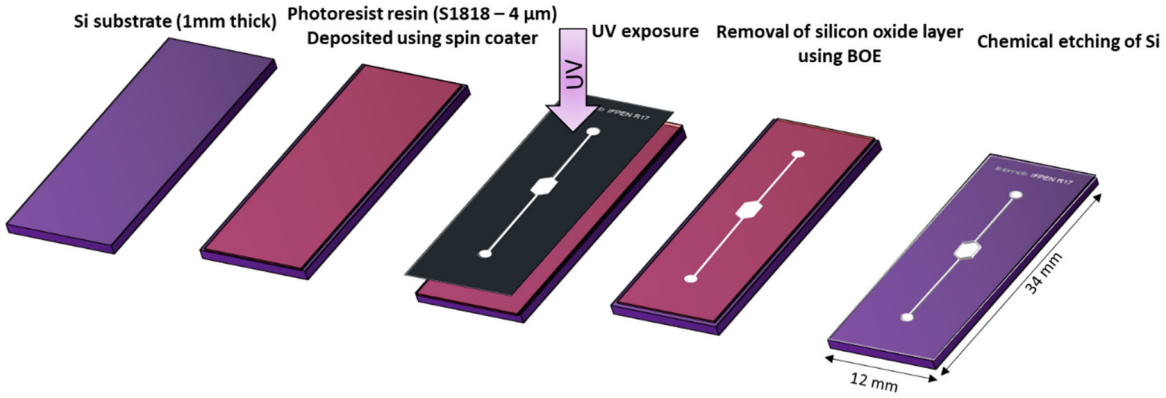

Figure ESI-1-1 :Illustration of photolithography steps used for microchannels fabrication.

***Sensor fabrication process*.** The sensor device consists of a metallic spiral geometry and square contact pads deposited on a borosilicate glass substrate (Borofloat 33, Schott). Platinum (Pt) was selected as the metal of choice because of its chemical inertia, its resistance to the thermal treatments, being physically and chemically stable, and allowing high accuracy temperature sensing [2,3]. The Pt film is deposited on the borosilicate substrate using a bi-layer photolithography process using two resin layers: a non-photosensitive resin (Lift-Off Resists, LOR) layer and a photoresist layer, which is used as a sacrificial layer for the deposition. This technique allows accessing high resolution and high aspect ratio structures [4]. The process starts with the use of a borosilicate glass substrate spin-coated with LOR resin from Micro Chem Corp at 750 rpm for 45 s, allowing the layer to spread out to a thickness of 0.7 µm. The substrate is placed on a hot plate, and the resin undergoes a baking step for 3 min at 150°C. Then, the same steps with the same operating parameters mentioned above are used to pattern the photoresist layer (spin coating, UV exposure, development…). At this stage, the pattern is developed in the two layers (the LOR and the photosensitive resin). The cross-section illustration after the UV exposure and development is presented Figure ESI-1-2. An undercut between the polymer LOR and the resin is formed, which is a key parameter to ensure the high resolution of the spiral geometry [5]. After the bi-layer photolithography, the metal deposition of thin films is performed using magnetron sputtering [6] using a Plassys MP450 system. Due to the lack of adhesion of the Pt on glass, we first deposited a Cr film adhesion layer of 5 nm, on the top of which a 200 ± 20 nm thick Pt film, is deposited to elaborate resistive elements in the ≈ 10^2 Ω range. The parameters used to perform the

deposition are the following: Argon as discharged gas with a pressure of 1 Pascal and 30W RF Power (13.56Mhz) with a deposition time of 40 min, the distance between the target and the substrate is fixed at 80 mm. After de deposition, the substrate is placed in a beaker and the photoresist resin is dissolved using a commercially available remover, N-Methyl-2-pyrrolidone (NMP) based solvent stripper designed for efficient photoresist resin removal (lift off process) along with the undesirable metallic deposited surface. Figure ESI-1-2 illustrates the steps followed during the bi-layer photolithography process.

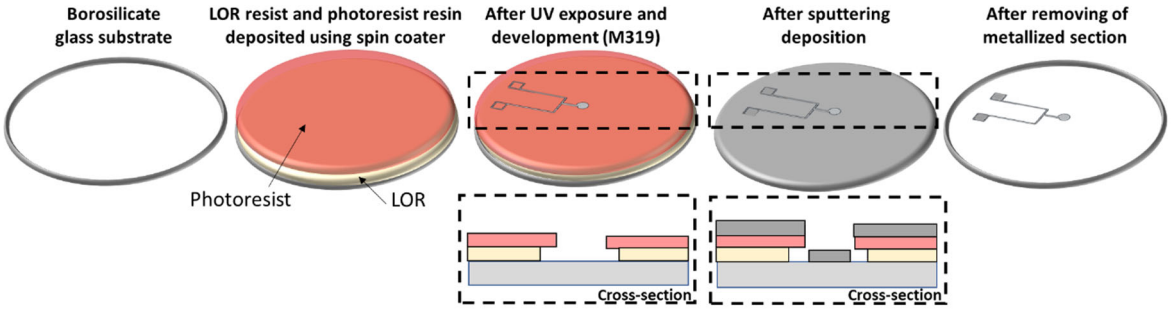

Figure ESI-1-2: Illustration of bi-layer photolithography steps used for sensor fabrication.

***Fusion bonding process*.** The silicon and glass substrates were assembled using a fusion bonding process. The bonding procedure started by cleaning the glass and silicon surfaces with isopropanol to avoid undesired contamination. Then both substrates were placed in air plasma cleaner model PDC-002 at 1000 W and 1,2 Torr for 10 min to activate the surface. The alignment of the substrate was performed with the help of an optical microscope by placing the spiral shaped sensor on the top of the micro-pool and then pressing them together, thereby initiating a pre-bonding process. The pre-bonded substrates were placed in an oven between two graphite sheets that allow a proper heat conduction, while preventing glass bonding to other materials (glass does not wet graphite). All the elements are placed on a ceramic plate, a weight is placed to apply a constant pressure on the assembly. The thermal treatment consists in reaching 700°C in 1 hour, followed by a 20-min plateau to initiate the creation of a melted diffusion layer at the interface. Then, an aging step at 600 °C is maintained for 5h. finally, a decreasing ramp at 5 °C/min down to 25 °C is performed.

ESI-2: Fluidic interfacing of the microfluidic device and λ measurement detailed.

The holder can incorporate temperature control through three heating cartridges placed in its body. The temperature is regulated using a K-type diameter (probe diameter: 0.3 mm) thermocouple placed as closed as possible of the Pt spiral sensor, between the holder and the microfluidic device, as shown in Figure ESI-2-1.

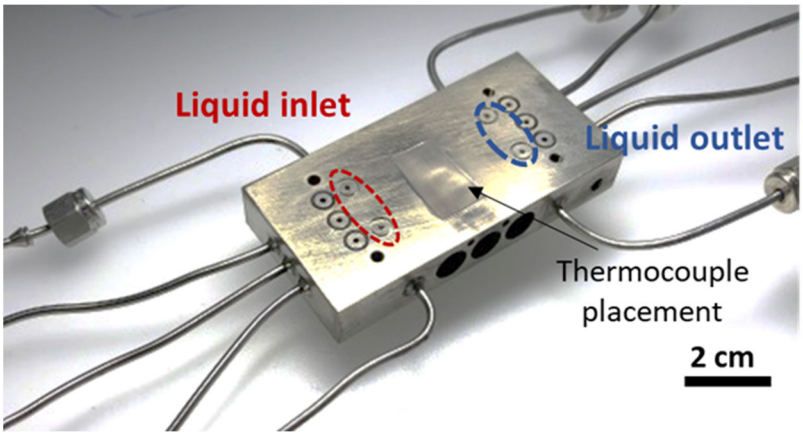

Figure ESI-2-1: View of the holder, the inlet and outlet channels are circled, and the arrow shows the thermocouple positioning.

Once the microfluidic device is placed in the holder, the electric interfaces are connected by means of square contact pads on both ends of the heater. The metallic sensor is connected to the electronic measurement device consisting of two spring loaded contact pins placed on the contact pads (Figure ESI-2-2).

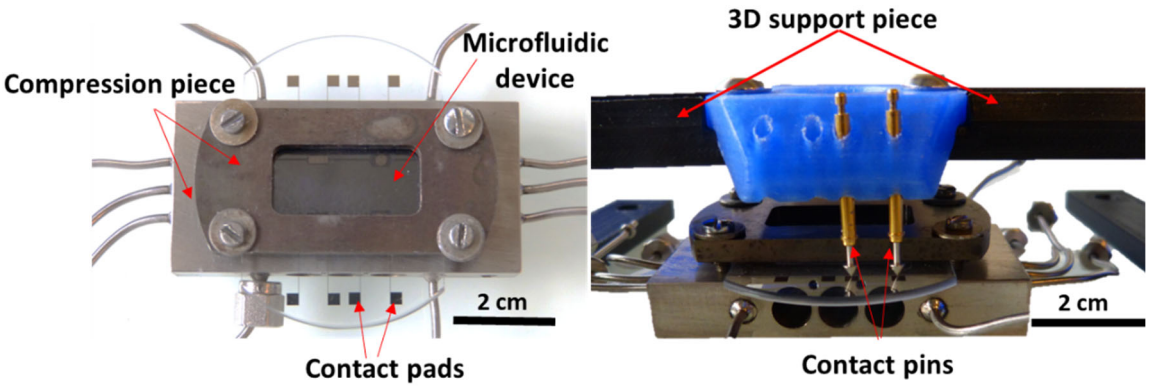

Figure ESI-2-2: Photo of the microfluidic device positioned and fixed in the holder. Photo of the support used to hold contact pins pressing against the contact pads.

ESI-3 : λ measurement detailed.

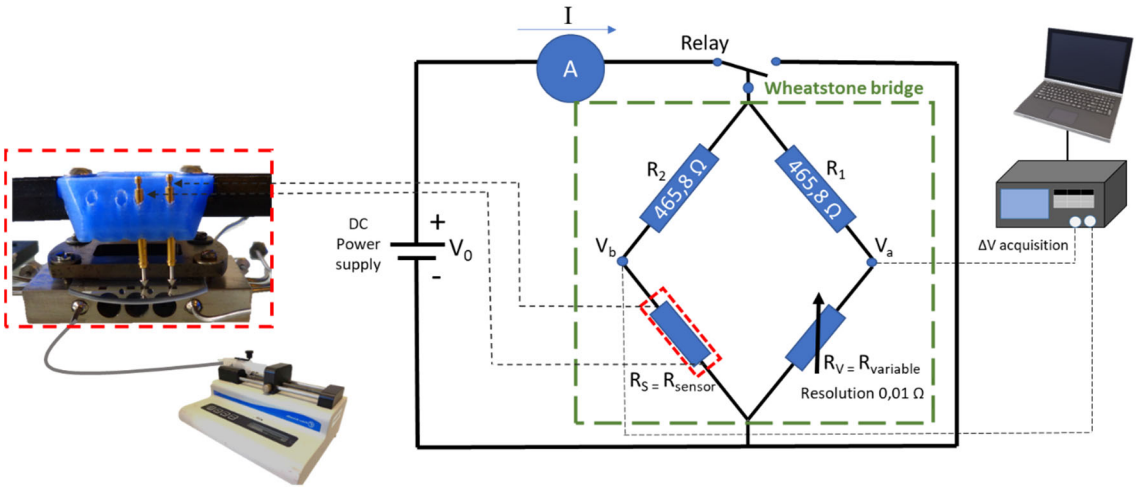

Figure ESI-3-1: Schematic of the λ measurement system.

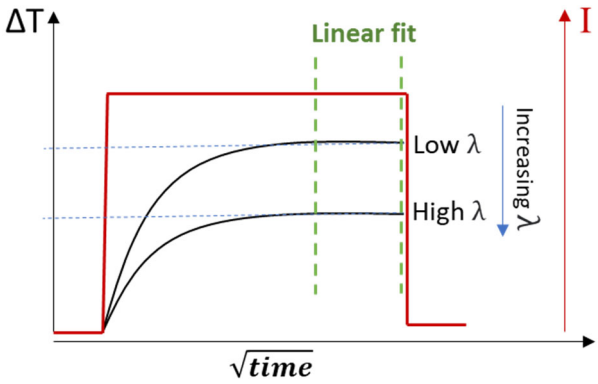

Figure ESI-3-2-: Simulated temperature response curves adapted from reference [7], showing that the offset of a linear regression at the end of a sensor response curve can be used to determine λ of a static fluid inside the microchannel.

ESI-4: Experimental references values and temperature response curves obtained for water/ethanol mixtures at different applied powers.

Table ESI 4-1: *Experimental reference values of thermal conductivity at 293.15 K for the fluids considered. The composition of mixtures is given in vol%.*

Fluids	λ (W/(m.K))	Ref.
ethanol	0.168	[8]
ethanol/water 75:25	0.286	[9]
ethanol/water 50:50	0.392	
ethanol/water 25:75	0.497	
water	0.603	[8]
n-pentadecane	0.137	[10]
ethane-1,2-diol	0.255	[11]

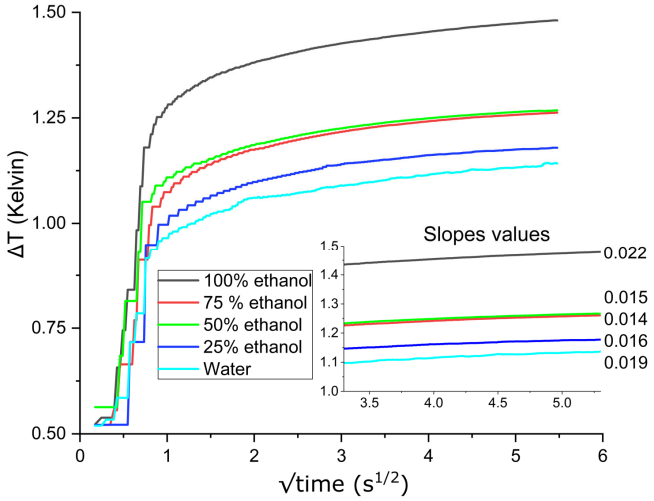

Figure ESI-4-1: Time variations of the temperature in the microcavity filled with water/ethanol mixtures when a heat pulse (30 mW during 30 s) is applied to the heater/sensor. The observed slopes are shown from a time interval of [3.3 $s^{1/2}$; 5.3 $s^{1/2}$].

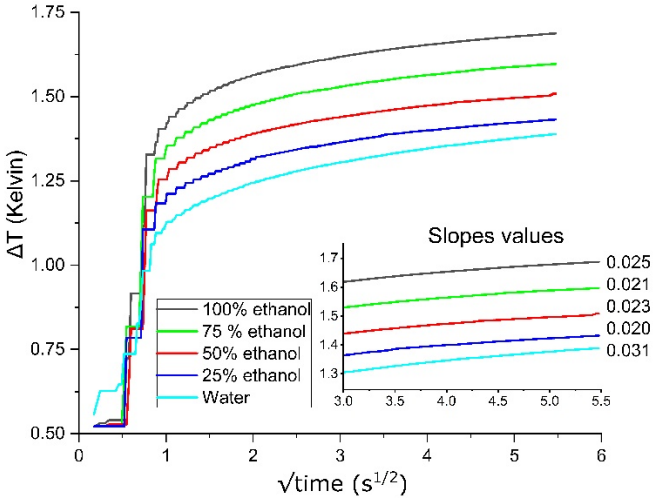

Figure ESI-4-2: Time variations of the temperature in the microcavity filled with water/ethanol mixtures when a heat pulse (40 mW during 30 s) is applied to the heater/sensor. The observed slopes values are shown from a time interval of [3.3 $s^{1/2}$; 5.3 $s^{1/2}$]

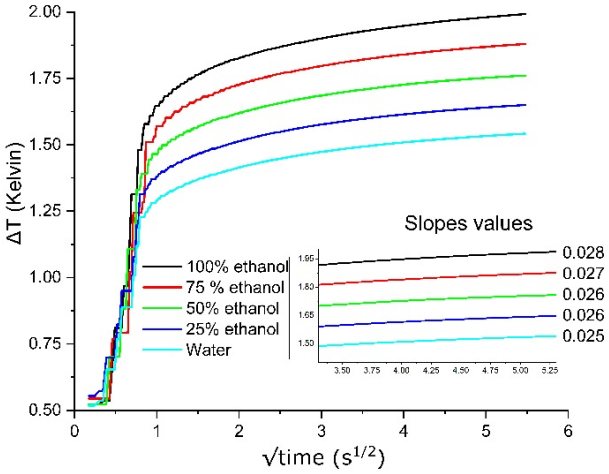

Figure ESI-4-3: Time variations of the temperature in the microcavity filled with water/ethanol mixtures when a heat pulse (50 mW during 30 s) is applied to the heater/sensor. The observed slopes values are shown from a time interval *of* [3.3 $s^{1/2}$; 5.3 $s^{1/2}$].

ESI-5: Calibration curve for λ measurement, parameters a and b and values measured for the three sensors

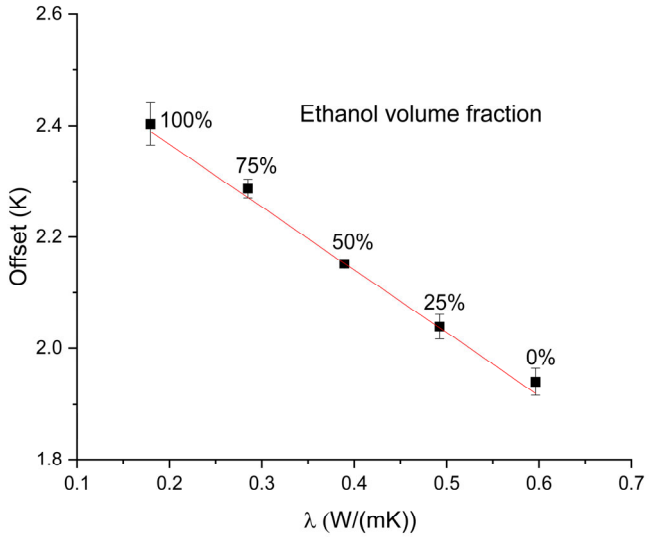

Figure ESI-5-1: Illustration of a calibration curve plotting the offset values (ΔT) resulting from fittings as a function of reference λ values for corresponding water/ethanol mixtures.

Table ESI-5-1: Values of the a and b parameters obtained for the calibration curve for each of the three sensors.

	a (K^2m/W)	b (K)
Sensor 1	-1.485 ± 0.078	2.819 ± 0.022
Sensor 2	-1.126 ± 0.061	2.591 ± 0.024
Sensor 3	-1.138 ± 0.056	2.596 ± 0.024

Table ESI-5-2: λ (W/(m.K)) values measured for the n-pentadecane and ethan-1,2-diol using the three sensors, at 293.15 K.

	n-pentadecane	ethan-1,2-diol
Theorical value	0.137 ± 0.007	0.255 ± 0.008
λ1	0.128 ± 0.010	0.290 ± 0.029

$\lambda 2$	0.138 ± 0.027	0.316 ± 0.015
$\lambda 3$	0.138 ± 0.004	0.300 ± 0.026
$<\lambda>$	0.134 ± 0.019	0.303 ± 0.028

References

[1] S. Marre, A. Adamo, S. Basak, C. Aymonier, K.F. Jensen, Design and Packaging of Microreactors for High Pressure and High Temperature Applications, Ind. Eng. Chem. Res. 49 (2010) 11310–11320. https://doi.org/10.1021/ie101346u.

[2] H. Darrell, Evaluating Thin Film RTD Stability, Sensors-the Journal of Applied Sensing Technology 14, no. 10, 1997.

[3] W.A. Clayton, Thin-film platinum for appliance temperature control, IEEE Trans. on Ind. Applicat. 24 (1988) 332–336. https://doi.org/10.1109/28.2875.

[4] M. Hatzakis, B.J. Canavello, J.M. Shaw, Single-Step Optical Lift-Off Process, IBM J. Res. & Dev. 24 (1980) 452–460. https://doi.org/10.1147/rd.244.0452.

[5] Y. Chen, A lift-off process for high resolution patterns using PMMA/LOR resist stack, Microelectronic Engineering 73-74 (2004) 278–281. https://doi.org/10.1016/j.mee.2004.02.053.

[6] S. Swann, Magnetron sputtering, Physics in Technology 19 (1988) 67–75. https://doi.org/10.1088/0305-4624/19/2/304.

[7] G. Oudebrouckx, D. Nieder, T. Vandenryt, S. Bormans, H. Möbius, R. Thoelen, Single element thermal sensor for measuring thermal conductivity and flow rate inside a microchannel, Sensors and Actuators A: Physical 331 (2021) 112906. https://doi.org/10.1016/j.sna.2021.112906.

[8] D. R. Lide, CRC handbook of chemistry and physics, 81st ed. (CRC, New York 2000).

[9] A.O. Guimarães, F.A.L. Machado, E.C. da Silva, A.M. Mansanares, Thermal Effusivity and Thermal Conductivity of Biodiesel/Diesel and Alcohol/Water Mixtures, Int J Thermophys 33 (2012) 1842–1847. https://doi.org/10.1007/s10765-012-1280-3.

[10] Bogatov, G.F., Rastorguev, Yu.L., Grigor'ev, B.A., Khim. Tekhnol. Topl. Masel, 14, 9, 31 (1969).

[11] L. Riedel, Forsch. Geb. Ing. Wes., 11, 6, 340 (1940).